frontiers in Materials

ORIGINAL RESEARCH
published: 13 April 2021
doi: 10.3389/fmats.2021.661104

Intelligent Hydrogel Actuators With Controllable Deformations and Movements

Qian Zhao, Zhenglei Yu, Yunhong Liang, Lei Ren and Luquan Ren*

The Key Laboratory of Bionic Engineering, Ministry of Education, Jilin University, Changchun, China

Near infrared laser- (NIR-) driven intelligent hydrogel actuator systems including printable N-isopropylacrylamide- (NIPAm-) nanosized synthetic hectorite clay-nanofibrillated cellulose (NFC) hydrogels and NIPAm-4-hydroxybutyl acrylate- (4HBA-) NFC hydrogels with a high response rate were prepared via three-dimensional (3D) printing and hydrothermal synthesis, respectively. The addition of NFC was beneficial to the improvement in rheology. The 3D printed intelligent hydrogel actuators with a structure pattern of Model I and Model II exhibited the saddle and inverted saddle deformations, respectively, to prove the validity of 3D printing. In order to improve the response rate and enrich movement patterns, the hydrothermal synthesized intelligent hydrogel actuators were prepared on the base of the 3D printed intelligent hydrogel compositions. The addition of NFC maintained the controllable NIR response. Based on a wedge-shaped design, the hydrothermal synthesized intelligent hydrogel pushed the resin ball with weight of 130 mg forward 8 mm in 39 s. By changing the torque values of a hydrogel in a different direction, the actuator realized controllable continuous rollover movement. Attributed to the longilineal shape, the intelligent hydrogel actuator reached an effective displacement of 20 mm in 10 s via a forward movement. The characteristics and structure design of a hydrogel material significantly realized multiple controllable functional four-dimensional (4D) printed deformations and movements. The combination of advantages of the 3D printed and hydrothermal synthesized intelligent hydrogels provided a new direction of development and abundant material candidates for the practical applications of 4D printing in soft robot, information sensing, and health engineering.

Keywords: 4D printing, intelligent hydrogel, nanofibrillated cellulose, near infrared laser response, controllable movement

OPEN ACCESS

Edited by:
Yusheng Shi,
Huazhong University of Science and Technology, China

Reviewed by:
Tongqing Lu,
Xi'an Jiaotong University, China
Shaoxing Qu,
Zhejiang University, China
Yan Zhou,
China University of Geosciences Wuhan, China

****Correspondence:***
Yunhong Liang
liangyunhong@jlu.edu.cn

Specialty section:
This article was submitted to Smart Materials, a section of the journal Frontiers in Materials

Received: *30 January 2021*
Accepted: *08 March 2021*
Published: *13 April 2021*

Citation:
Zhao Q, Yu Z, Liang Y, Ren L and Ren L (2021) Intelligent Hydrogel Actuators With Controllable Deformations and Movements. Front. Mater. 8:661104. doi: 10.3389/fmats.2021.661104

INTRODUCTION

With the development of materials and equipment manufacturing technology, intelligent materials and corresponding advanced preparation methods promote the integrative development of materials, mechanics, and information (Zhang et al., 2014; Hakan et al., 2016; Wang et al., 2018). By stimulation of temperature (Gladman et al., 2016), light (Wang et al., 2013), electricity (Must et al., 2015), and humidity (Xue et al., 2015), intelligent materials own the basic shape variation property. The soft intelligent materials in combination with a specific structure design can realize controllable deformation and movements, which enrich the material candidates of (four-dimensional) 4D printing in the field of application of soft actuator, artificial muscle, etc.

As a kind of typical soft intelligent materials, intelligent hydrogels possess the swelling and deswelling properties initiated by stimulating on the base of a three-dimensional (3D) net structure. Attributed to the outstanding biocompatibility, intelligent hydrogels have been used in the practical applications of soft actuator, electron device, and medical appliance (Liu et al., 2017). Attributed to the characteristics of non-invasive safety (Jiang et al., 2014) and non-contact control (Weissleder, 2001), a near infrared laser (NIR) of 808 nm is one type of convenient common stimulation methods. The addition of a photothermal conversion agent, including graphene oxide (GO) (Fujigaya et al., 2008), carbon nanotube (Lu and Panchapakesan, 2007), gold nanoparticle (Lo et al., 2011), etc., into a hydrogel matrix is a key point for a laser-driven property of hydrogels. Based on the volume shrinkage response, NIR-driven intelligent hydrogels own bending/unbending deformation property. Intelligent hydrogels in combination with a structure design own the swimming, capturing, and crawling (Wang et al., 2015; Yao et al., 2015; Hu et al., 2017) movement properties. Considering a significance of the application of the deformation and movement, the response rate is a basis for the functional requirement of continuous movement of intelligent hydrogels. Attributed to the crosslinking patterns and a relatively low swelling/deswelling rate, the existing NIR-driven intelligent hydrogels including 3D printed hydrogels exhibit a relatively low response rate, which restricts functional movement abilities. Therefore, the question of how to improve the response rate and balance mechanical strength is a key point for the functional application of the 4D printed intelligent hydrogels.

Many researches focused on the enhancement of functional movement properties of intelligent hydrogels including the manipulation of material components and a structure design. Luo et al. (2015) prepared a kind of gradient temperature-responsive hydrogel via the heterobifunctional crosslinker of 4-hydroxybutyl acrylate (4HBA), which realized a relatively high swelling/deswelling rate. By using polypyrrole nanoparticles as photothermal transducers, the prepared hydrogel exhibited a high NIR response rate. However, the relatively low mechanical strength and single Young's modulus value further restricted the functional applications. In our previous studies (Zhao et al., 2018b,c), the nanofibrillated cellulose (NFC) exhibited an excellent role of the mechanical strength reinforcement in poly-N-isopropylacrylamide- (NIPAm-) nanosized synthetic hectorite clay hydrogels prepared via molding and 3D printing. Moreover, in addition to relatively high mechanical strength, the prepared NFC-reinforced gradient intelligent hydrogels own a relatively high response rate, multiple response patterns, and diversified self-driven functions under the stimulation of NIR (Zhao et al., 2018b, 2020), which realizes a perfect balance between the strength and response rate. The infiltration of GO in a hydrogel matrix realized an efficient NIR response. Even though the NFC-reinforced intelligent hydrogels realized the 3D printing and function properties, the effect of NFC content on the rheology characteristics of the 3D printed hydrogel reaction mixture and on movement patterns especially the controllable functional movement properties of the hydrothermal synthesized hydrogels should be further investigated.

Facing the requirements of a 4D printing developing application, two kinds of hydrogel system including 3D printed intelligent hydrogel actuator and hydrothermal synthesized intelligent hydrogel actuator were prepared. As the reinforcement, the effect of NFC content on rheology and printable ability of the 3D printed hydrogel reaction mixtures was investigated. The NFC-reinforced hydrothermal synthesized intelligent hydrogels, in combination with entirety infiltration of GO, were prepared to further extend the corresponding functional movement patterns. Moreover, the mechanisms of movement were also explained via an analysis of mathematics and mechanics.

EXPERIMENTAL SECTION

Materials

Intelligent hydrogels were synthesized via the monomer of NIPAm (Aladdin, Shanghai, China, 2% stabilizer), a crosslinking agent of the nanosized synthetic hectorite clay [Laponite XLG, $Mg_{5.34}Li_{0.66}Si_8O_{20}(OH)_4$, Rockwood, Ltd., Geesthacht, Germany], and 4HBA (J&K Scientific, Ltd., Beijing, China), a reinforcement of NFC without carboxyl (Guilin Qihong Technology Co., Ltd., Guilin, China), an initiator of ammonium persulfate [APS, $(NH_4)_2S_2O_8$, Sinopharm Chemical Reagent Co., Ltd., Shanghai, China] and potassium peroxydisulfate [KPS, $K_2S_2O_8$, Shanghai Aibi Chemical Reagent Co., Ltd., Shanghai, China, analytical reagent (AR)], and a catalyst of N,N,N′,N′-tetramethylethylenediamine (TEMED, Tianjin Weiyi Chemical Technology Co., Ltd., Tianjin, China, 98%). GO (Suzhou Hengqiu Graphene Technology Co., Ltd., Suzhou, China) was treated as a photothermal conversion agent and used as normal. Pure water (resistivity ≥18.2 MΩ·cm) was obtained by deionization and filtration.

Preparation of 3D Printed Intelligent Hydrogel Actuator

In order to prepare a hydrogel reaction mixture with GO, GO dispersed in pure water by ultrasonic radiation for 30 min and stirred for 1 h via a magnetic stirrer (Model MS-H380-Pro, DLAB Scientific Co., Ltd., China). Then, XLG clay was added and stirred for 1 h. Then, NFC with different weights was added and stirred for 1 h in an ice-water bath. Then, NIPAm was added into miscible liquids of GO, XLG, and NFC and stirred for another 2 h. Finally, KPS solution and TEMED were added under stirring. The hydrogel composition for 3D printing is listed in **Table 1**. Based on our previous study (Zhao et al., 2018a), GO content of 2 mg/ml exhibited maximum photothermal conversion efficiency, which was adopted in this experiment. Attributed to the NFC content, the hydrogel reaction mixtures were named as GO2-NFC0, GO2-NFC8, GO2-NFC9, GO2-NFC10, GO2-NFC11, and GO2-NFC12, respectively. After the preparation of a hydrogel reaction mixture for 3D printing, the.STL files were generated from Solidworks ad sliced by Slic3r software39. After 3D printing via a laboratory-made 3D printer with a needle of 20 G, the printed samples were placed in a vacuum dryer immediately at room temperature for *in situ* free radical polymerization under vacuum. A preparation process of the 3D printed intelligent

TABLE 1 | Compositions of intelligent hydrogel reaction mixture for three dimensional (3D) printing.

Reaction mixture	NIPAm (g)	GO (mg)	NFC (mg)	XLG (g)	KPS (mg)	TEMED (μL)	H_2O (mL)
GO2-NFC0	1.13	20	0	0.349	10	5	10
GO2-NFC8	1.13	20	80	0.349	10	5	10
GO2-NFC9	1.13	20	90	0.349	10	5	10
GO2-NFC10	1.13	20	100	0.349	10	5	10
GO2-NFC11	1.13	20	110	0.349	10	5	10
GO2-NFC12	1.13	20	120	0.349	10	5	10

TABLE 2 | Compositions of hydrothermal synthesized intelligent hydrogels.

Sample	NFC (mg)	NIPAm (g)	APS (mg)	4HBA (μL)	H_2O (mL)
NFC0	0	1	10	210	10
NFC2	20	1	10	210	10

hydrogel actuators is shown in **Figure 1A**. The compositions are listed in **Table 1**.

Preparation of Hydrothermal Synthesized Intelligent Hydrogel Actuator

Nanofibrillated cellulose was added into 10 ml of pure water, which was degassed in a continuous nitrogen-saturated atmosphere and stirred for 0.5 h via a magnetic stirrer (Model MS-H380-Pro, DLAB Scientific Co., Ltd., Beijing, China) under the circumstances of ice-water bath. Then, NIPAm and APS were added into NFC aqueous solution and stirred for 1 h. Finally, 4HBA was added into the aqueous solution and stirred for 5 min. After the hydrothermal synthesis in a 200-ml reaction kettle under the circumstances of 190°C for 5 h, an intelligent hydrogel was successfully prepared. In order to realize different deformation and movement patterns, the hydrothermal synthesized intelligent hydrogel without NFC and with 2 mg/ml of NFC was prepared, and was named as NFC0 and NFC2, respectively. The compositions are listed in **Table 2**.

The GO aqueous solution with the concentration of 4 mg/ml was prepared for the GO infiltration of hydrothermal synthesized intelligent hydrogels. Based on the porous microstructure, the GO aqueous solution can be efficiently infiltrated into the hydrogels. Before the infiltration, a filter paper was repeatedly used to absorb the water in hydrogels. Then, the hydrogel entirety or the hydrogel block with specific dimensions was immersed into the GO aqueous solution and maintained for 5 min to finish entirety infiltration. The preparation and GO infiltration process of the hydrothermal synthesized intelligent hydrogel actuator can be observed in **Figure 1B**.

Characteristics of Intelligent Hydrogels

Microstructure

After freeze-drying (LGJ-10C, Beijing Four Ring Scientific Instrument Factory Co., Ltd., Beijing, China), the cross sections of the hydrothermal synthesized intelligent hydrogels were observed via field emission scanning electron microscopy (FESEM; Model XL-30, FEI Company, OR, USA) to disclose the characteristics of microstructure.

Infrared Spectroscopy and Differential Scanning Calorimetry

IRAffinity-1 Fourier transform infrared (FTIR) spectrometer (Shimadzu Corporation, Kyoto, Japan) was used to analyze the FTIR spectra characteristics of hydrothermal synthesized intelligent hydrogels. The wavenumber range was set as 500–4,000 cm^{-1}. The volume phase transition temperatures were tested via differential scanning calorimetry (DSC; Model DSC25-RCS90, TA Company, New Castle, DE, USA). The samples were heated from 10 to 60°C at a rate of 20°C/min under nitrogen atmosphere.

Young's Modulus

The ultrasound image diagnostic apparatus (Alxplorer, Supersonic Imagine, Aix-en-Provence, France) was used to test the values of Young's modulus of hydrothermal synthesized intelligent hydrogels. A SL15-4 probe was adopted to measure the full swollen hydrogels in water. Young's modulus can be directly obtained in the image.

Rheological Analysis

The rotational rheometer (DHR, TA Instruments, New Castle, DE, USA) with a parallel plate geometry of 40 mm in diameter and a gap of 0.55 mm was used to test the rheological properties of the 3D printed hydrogel reaction mixture. Strain sweeps in the range of 0.1–100% with frequencies of 0.1–2 Hz were used to determine the linear viscoelastic range.

Deformations and Movements of Intelligent Hydrogel Actuators

NIR Response Measurement of 3D Printed Intelligent Hydrogel Actuator

In order to analyze the effect of a structure design on deformation characteristics of the 3D printed hydrogel actuators, two kinds of structure pattern, which were named as Model I and Model II, were constructed. Model I was a cylindrical bilayer structure with 90°/0° configuration, owning a dimension of 30 mm in diameter, a thickness of 0.96 mm, and a filling rate of 100%. Model II was also a bilayer structure with the same dimensions of Model I. But the filamentary of Model II was arc. The bilayer constructed with

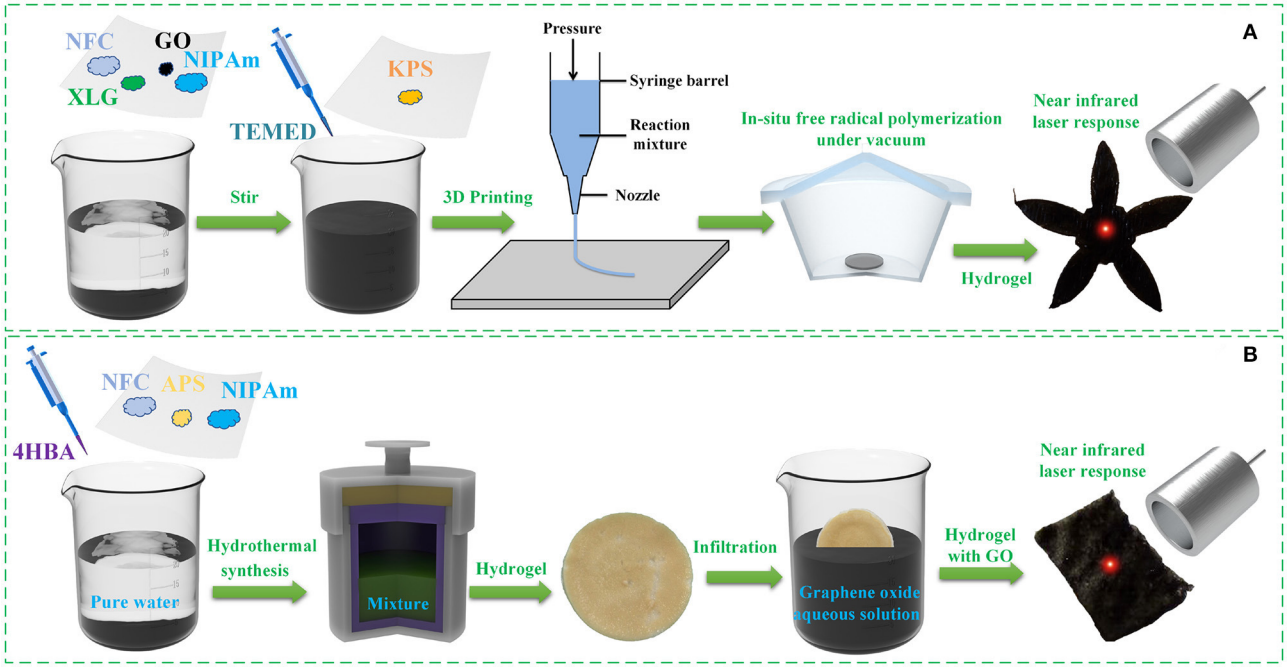

FIGURE 1 | Preparation schematic diagram of the **(A)** three-dimensional (3D) printed and **(B)** hydrothermal synthesized intelligent hydrogels with graphene oxide (GO).

arcs was also 90°/0° configuration. The 3D printed intelligent actuators with full swelling state were placed in water of room temperature. NIR with wavelength of 808 nm (Model FC-W-808-30W, Changchun New Industries Optoelectronics Technology Co., Ltd., Changchun, China) was treated as a source of stimulation. The deformation and movement processes were recorded by digital camera.

NIR Response Measurement of Hydrothermal Synthesized Intelligent Hydrogel Actuator

After the infiltration of GO, the wedge-shaped NFC2 intelligent hydrogel with dimensions of 12 mm × 3 mm × 4 mm (length × width × maximal thickness) was used to push the resin ball (Φ6 mm) with weight of 130 mg on a glass surface. The NIR power was 7.1 W.

After transitory infiltration of GO, the middle part of the NFC0 hydrogel block was adopted to realize the rollover movement. Attributed to the infiltration depth, GO particles existed in the outer surface of a sample. After cutting off two opposite outer surfaces, there were no GO particles in the middle part of the remaining strip sample with dimensions of 10 mm × 3 mm × 4 mm (length × width × thickness). The NIR with power of 7.1 W was irradiated on the middle part of a strip sample to realize the rollover movement.

After infiltration of GO, the bottom part of the NFC0 hydrogel with dimensions of 23 mm × 2 mm × 2 mm (length × width × thickness) was cutting off to exhibit the forward movement under the stimulation of NIR with power of 7.1 W.

RESULTS AND DISCUSSION

NIR Responses of 3D Printed Hydrogel Actuator

In order to prove the effect of NFC addition on printability of intelligent hydrogel reaction mixtures and disclose the optimal NFC content for 3D printing of intelligent hydrogel actuators, the rheology characteristics including apparent viscosity, storage modulus, and loss modulus are analyzed in **Figure 2**. The apparent viscosity in **Figure 2A** indicated that the hydrogel reaction mixtures owned shear thinning characteristic. The addition and variation of NFC content increased the apparent viscosity and changed variation tendency of a hydrogel reaction mixture. As shown in **Figure 2B**, the storage modulus and loss modulus of the hydrogel reaction mixtures with NFC were higher than those without NFC, which exhibited the gel-sol transition point in the strain range of 10^1-10^2%. The hydrogel reaction mixtures with NFC owned higher property of energy storage by elastic deformation and energy loss by viscous deformation, exhibiting perfect printability. The hydrogel with a relatively low NFC content owned a relatively high swelling kinetics characteristic (Zhao et al., 2018a,c). Considering the swelling and rheology, the GO2-NFC10 hydrogel reaction mixture was used for the 3D printed hydrogel actuators.

In situ free radical polymerization under vacuum realized the solidification of the 3D printed hydrogel actuators successfully with GO (Zhao et al., 2018a). Based on high printable property (**Supplementary Movie 1**), the 3D printed GO2-NFC10 hydrogel actuators with the structure of Model I and Model II after the polymerization exhibited controllable NIR deformations in

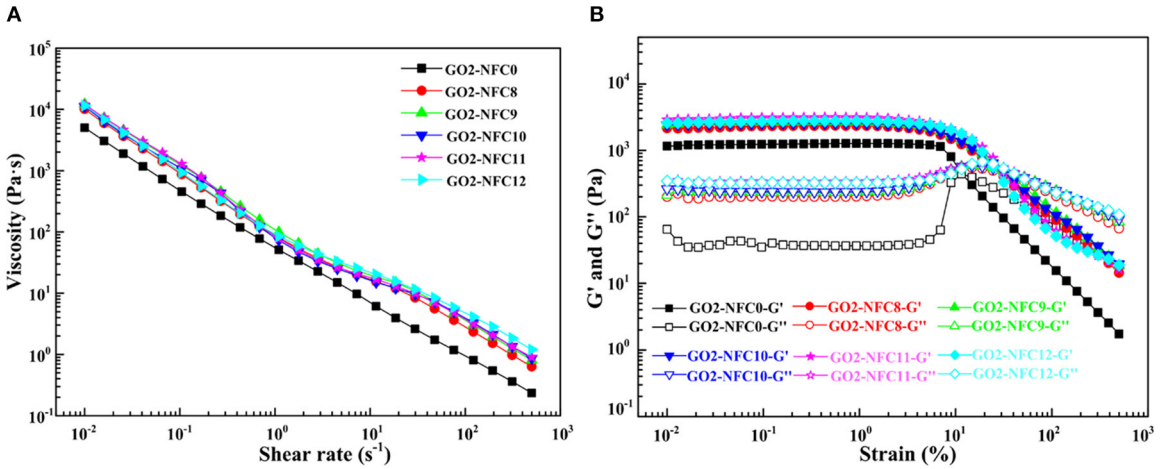

FIGURE 2 | (A) Apparent viscosity, **(B)** storage modulus G′ and loss modulus G″ of intelligent hydrogel reaction mixtures with GO.

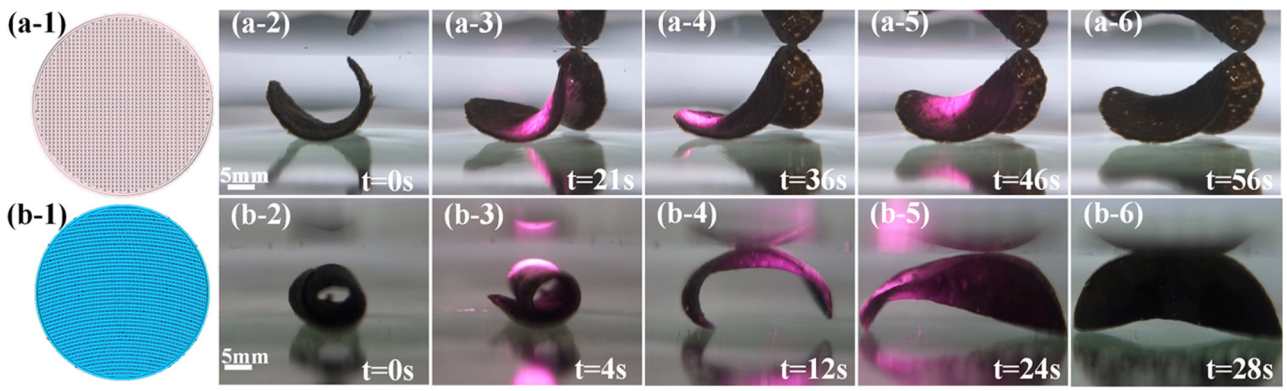

FIGURE 3 | Near infrared laser (NIR) responses of the 3D printed hydrogel actuators with **(a-1)**–**(a-6)** Model I and **(b-1)**–**(b-6)** Model II structures.

Figure 3. **Figure 3a-1** shows the structure pattern of Model I. In the initial state of **Figure 3a-2**, Model I exhibited a cincinal shape. When the NIR laser irradiated the right part, left part, and middle part in a sequence, the corresponding parts unfolded and rose, as shown in **Figures 3a-3–a-5**. After irradiation, Model I exhibited the final state of saddle in **Figure 3a-6**. The deformation process of Model I was exhibited in **Supplementary Movie 2**. **Figure 3b-1** shows the structure pattern of Model II. The initial state of Model II exhibited a hollow cylindrical shape in **Figure 3b-2**. Under the NIR irradiation, the right and left parts unfolded in a sequence, as shown in **Figures 3b-3–b-5**. The final state of Model II was an inverted saddle in **Figure 3b-6**. The deformation process of Model II was exhibited in **Supplementary Movie 3**. Based on a different printing structure, Model I and Model II owned a different deformation process and pattern.

The polymerization and structure were the key points for intelligent deformation of 3D printing of hydrogel actuators. The anisotropic swelling/deswelling behavior of a printed structure built a base of the deformation mechanism of the 3D printed hydrogel actuators. Even though the 3D printed hydrogel actuator realized precise structure patterns and controllable intelligent deformation, the deformation patterns were restricted by the response rate of hydrogel materials. Therefore, in order to improve the response rate of a hydrogel actuator and realized multiple deformation and movement patterns, a crosslinking agent was changed from XLG to 4HBA on the base of the 3D printed hydrogel compositions. The regulatory material composition provided a new method for the improvement and application of the 4D printed hydrogel actuators.

NIR Responses of Hydrothermal Synthesized Hydrogel Actuator

Material Characteristics

Figure 4 shows the microstructure characteristics of NFC0 and NFC2. Based on the micropore size variation scale, NFC0 can be divided into four layers (including Layer 1, Layer 2, Layer 3, and Layer 4) qualitatively, which exhibited a gradient structure. From Layer 1 to Layer 4, micropore size decreased gradually along with the thickness direction, as shown in

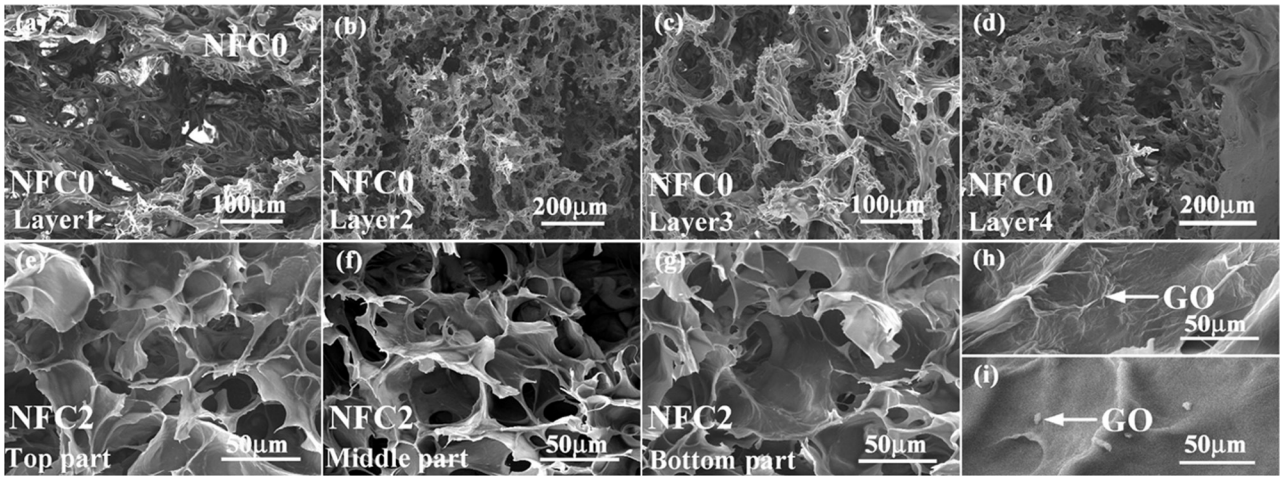

FIGURE 4 | Microstructure characteristics of different parts in **(a–d)** nanofibrillated cellulose 0 (NFC0), **(e–g)** NFC2 and GO distribution patterns in **(h)** the top and **(i)** middle parts of NFC2.

Figures 4a–d. The addition of NFC significantly affected the microstructure characteristics of the NFC2 intelligent hydrogel, which weaken the original gradient structure. The NFC2 hydrogel was divided into bottom part, middle part, and top part, as shown in **Figures 4e–g**. Because of the existence of NFC and corresponding amount, convex structure existed on micropore surfaces of the NFC2 hydrogel. The addition of reinforcement maintained the infiltration property of the NFC2 hydrogel. Attributed to the infiltration method, the infiltrated GO amount was different between the top part and middle part of the NFC2 hydrogel. The synthesized mechanisms of the NFC0 and NFC2 intelligent hydrogels can be explained (Zhao et al., 2020). As the monomer and crosslinking agent, the addition reaction of double bond occurred between NIPAm and 4HBA, leading to the polymer with a hydroxide radical (PNIPAm-4HBA-OH). In the sediment process of synthesized polymers, the dehydration synthesis existed in hydroxide radical, forming a gradient network structure of NFC0. NFC owned another role of crosslinking agent in the material system. Because of the existence of hydroxide radical in NFC, the dehydration synthesis of hydroxide radical of NFC, and polymer with hydroxide radical (PNIPAm-4HBA-OH) via the addition reaction led to the existence of a relatively homogeneous network structure in NFC2. The typical network structure of NFC0 and NFC2 built the functional material base of hydrogel actuators. Moreover, the difference in the microstructure characteristics of NFC0 and NFC2 provided selective materials for hydrogel actuators with different functional applications.

Attributed to the Young's modulus range (1.2–2.7 KPa) in **Figure 5a**, NFC0 hydrogel can be divided into four layers, which was similar to the microstructure partition pattern in **Figures 4a–d**. As shown in **Figure 5b**, the maximum Young's modulus of the NFC2 hydrogel was 11.3 KPa, indicating that the addition of NFC increased the corresponding Young's modulus. In addition to the higher Young's modulus, the thickness of the NFC2 hydrogel was lower than that of the NFC0 hydrogel. Based on the variation in Young's modulus, NFC realized the reinforcement role in a hydrogel material system, which provided a selective base for the driving force of hydrogel actuators.

Fourier transform infrared analysis of the NFC0 and NFC2 hydrogels are shown in **Figure 6**. The band between 3,200 and 3,600 cm^{-1} represented N-H stretching vibration peaks. The band at 1,655 cm^{-1} was the C=O stretching vibration peak. The band at 1,548 cm^{-1} was assigned to the N-H bending vibration peak. The bands at 1,381 and 1,456 cm^{-1} represented the absorption peaks of $-CH(CH_3)_2$, respectively. The hydrophilic acylamino and the hydrophobic isopropyl existed in the intelligent hydrogels. The functional chemical bonds of NIPAm were maintained in the NFC2 hydrogel, which built a functional base of NIR responses for controllable hydrogel actuators.

Fourier transform infrared disclosed the temperature response functional base of the NFC0 and NFC2 hydrogels. **Figure 6** shows the corresponding volume phase transition temperature (VPTT) of NFC0 (37.8°C) and NFC2 (35.3°C), respectively. The results of DSC were similar to the results of FTIR. The addition of NFC maintained the temperature response behavior of hydrogels. The NFC0 and NFC2 intelligent hydrogels, in combination with an analysis of microstructure, Young's modulus, FTIR, and DSC, owned the intelligent temperature response property base. Based on the infiltration of GO, the prepared intelligent hydrogels can realize NIR responses. In combination with a structure design, the controllable functional movements of hydrogels can also be obtained.

Controllable Movement Characteristics

Pushball Movement

Figures 4–6 indicated that the NFC0 and NFC2 hydrogels owned the intelligent deformation properties from a material point of view. In combination with a structure design, the NFC0 and NFC2 hydrogel actuators with the GO infiltration possessed

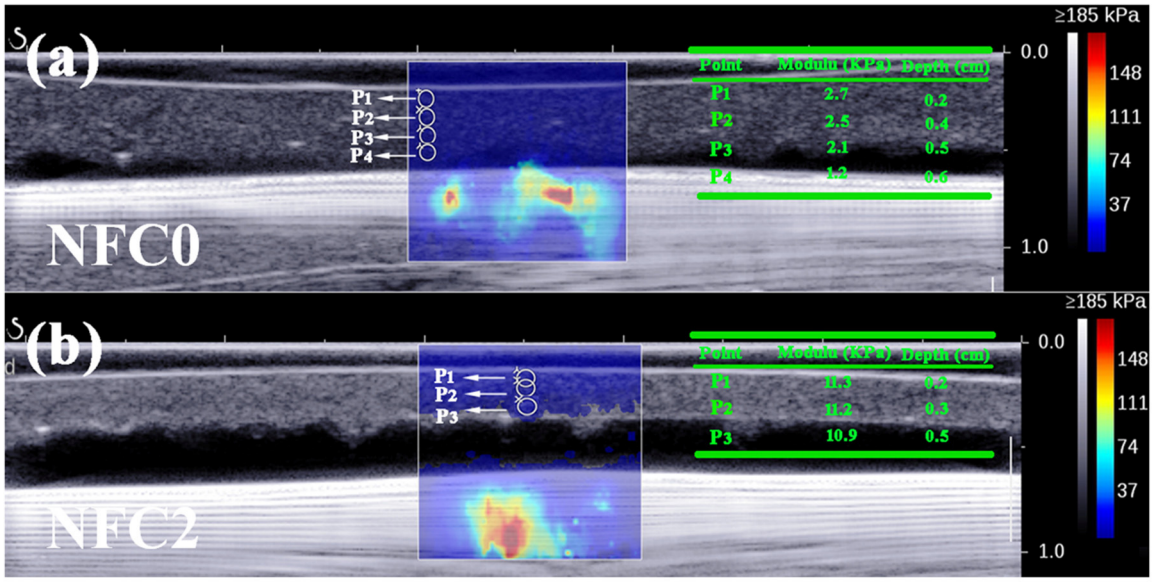

FIGURE 5 | Distribution characteristics of Young's modulus of the **(a)** NFC0 and **(b)** NFC2 intelligent hydrogels.

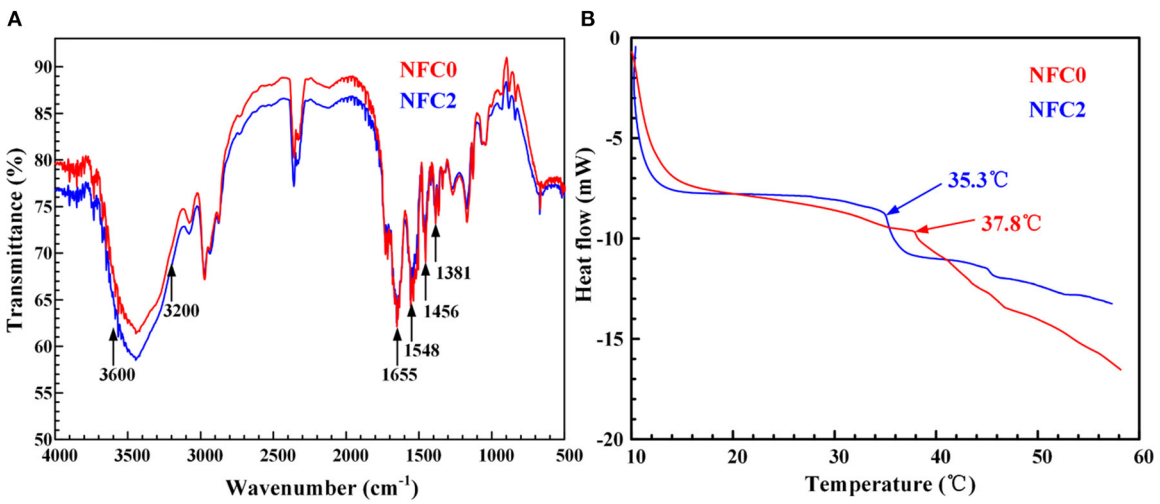

FIGURE 6 | (A) Typical Fourier transform infrared (FTIR) spectra and **(B)** differential scanning calorimetry (DSC) curves of the NFC0 and NFC2 intelligent hydrogels.

controllable movement properties under the stimulation of NIR from a point view of function application.

The NFC2 hydrogel actuator with a wedge-shaped structure having GO was designed to conduct the pushball movement, as shown in **Figure 7**. The hydrogel actuator used for the pushball movement was cut into a wedge shape first, and then infiltrated GO. **Figure 7a** exhibits the original position of the hydrogel actuator and resin ball. After infiltration, a part of the hydrogel actuator exhibited black. Based on Young's modulus distribution characteristics of the NFC2 hydrogel and perviousness of NIR, the bottom part of the NFC2 hydrogel was treated as the top part of the actuator to ensure the NIR contact of the middle part of the NFC2 hydrogel and bending deformation of the NFC2 hydrogel actuator. NIR irradiated on the middle part of the NFC2 hydrogel actuator, which led to the contraction deformation in **Figure 7b**. After removing NIR irradiation, the NFC2 hydrogel actuator conducted extension deformation and reached the original straight state. Attributed to the weight distribution of wedge shape, the right part of the NFC2 hydrogel actuator acted as a fulcrum role, driving the actuator forward in **Figure 7c**. In the first distance, the resin ball was pushed forward about 2 mm. The pushball movement of the NFC2 hydrogel actuator was repeatable. By repeating NIR irradiation, the actuator moved another

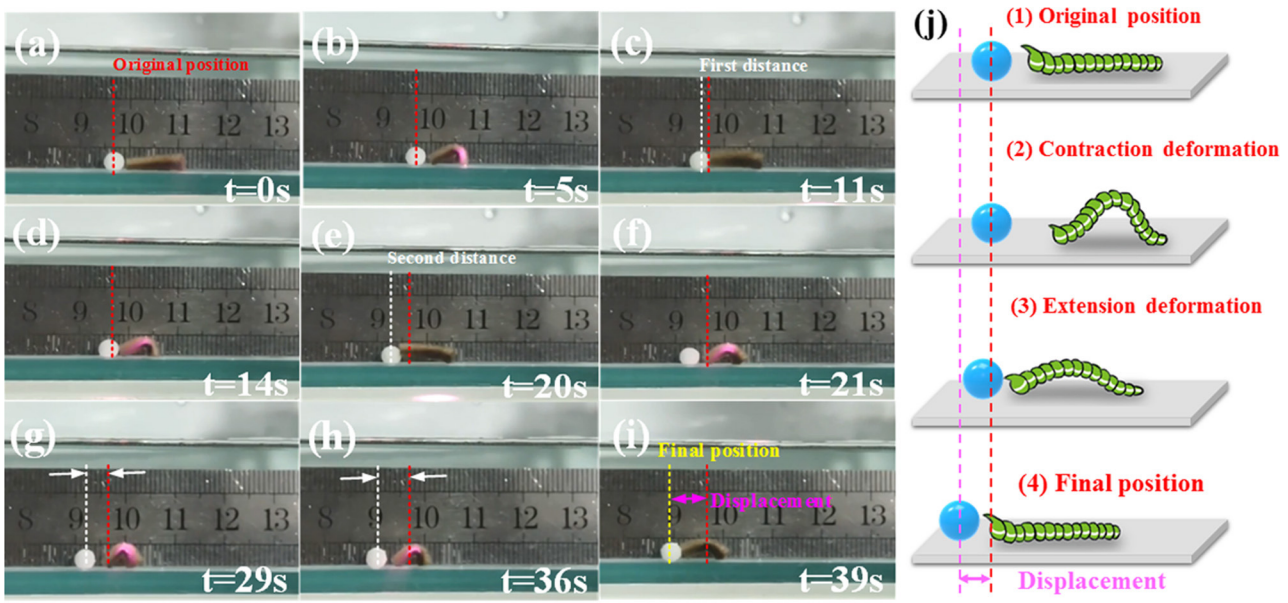

FIGURE 7 | The **(a–i)** multiple repetitive process and **(j)** displacement schematic diagram of pushball movement. Arrow represents the boundary of displacement.

four steps in 15 s. The resin ball was pushed four distances correspondingly, as shown in **Figures 7d–i**. The vivid movement can be observed in **Figure 7j** and **Supplementary Movie 4**. Compared with the original position and final position, the effective displacement of pushball movement was 8 mm in 39 s, which exhibited a controllable movement characteristic of NFC2 hydrogel actuators.

The swelling/deswelling property and artful structure designs were the key points for NIR-driven pushball movements, on the base of GO infiltration. Relatively high Young's modulus restricted the movement rate and improved the driving force to some extent. In the pushball movement process, the movement of resin ball was independent of the hydrogel actuator deformation. The hydrogel actuator contacted with a resin ball via the driving force in extension deformation, leading to the corresponding forward displacement along with the movement direction of the NFC2 hydrogel actuator.

Rollover Movement

Figure 8 exhibits the rollover movement process of the NFC0 intelligent hydrogel actuator. **Figure 8a** shows the initial state of a hydrogel actuator. After the infiltration and ordered cutting, GO particles existed in the specific four sides. NIR irradiated the middle part of the hydrogel actuator, which induced the volume shrinkage of the middle part. Under continuous NIR irradiation, the irradiated long side of the hydrogel actuator switched to another long side direction. When the NIR irradiated another long side, the irradiated long side continued the rollover movement, which formed a continuous rollover movement, as shown in **Figures 8b–e**. After removing the NIR irradiation, the NFC0 hydrogel actuator returned to the initial state, as shown in **Figure 8f**. A reversible and repeatable rollover movement process can be observed in **Supplementary Movie 5**. In our previous study (Zhao et al., 2020), the curvature variation was selected to build relationships of bending degree, deformation displacement, material properties, and incentive intensity on the base of mechanical analysis to disclose the self-driven mechanisms of hydrogel actuators. Moreover, based on the Foppl–von Karman elastic theory, the relationship between the curvature of the hydrogel actuator on x-axis and y-axis and the NIR power was constructed. By using the Rayleigh–Ritz method, the NIR power intensity value directly affected the longitudinal and transverse curvatures. With an increase in the NIR power, the relationship between the longitudinal and transverse curvatures changed from equality to inverse. Different NIR power densities affected the torque values of intelligent hydrogel actuators on x-axis and y-axis, respectively. Therefore, when the NIR power reached a specific value, the variation between the longitudinal and transverse curvatures affected the torque values (M_{xx} and M_{yy}) of the NFC0 hydrogel actuator on the stated x-axis and y-axis and realized a rollover movement, as shown in **Figure 8g**.

Forward Movement

Figure 9 shows the forward movement characteristics of the NFC0 intelligent hydrogel actuator. The initial state of the hydrogel actuator was straight strip in **Figure 9a**. As shown in **Figure 9b**, under the NIR irradiation, the middle part of the NFC0 hydrogel actuator exhibited a bending deformation. When the actuator reached the minimum bending degree, the NIR was removed. The middle part of the actuator moved forward about 13 mm in **Figure 9c**. Even though the actuator moved back in the extension process, the whole actuator moved forward about 9 mm in **Figure 9d**. The forward movement was repeatable. Compared with the original position, after

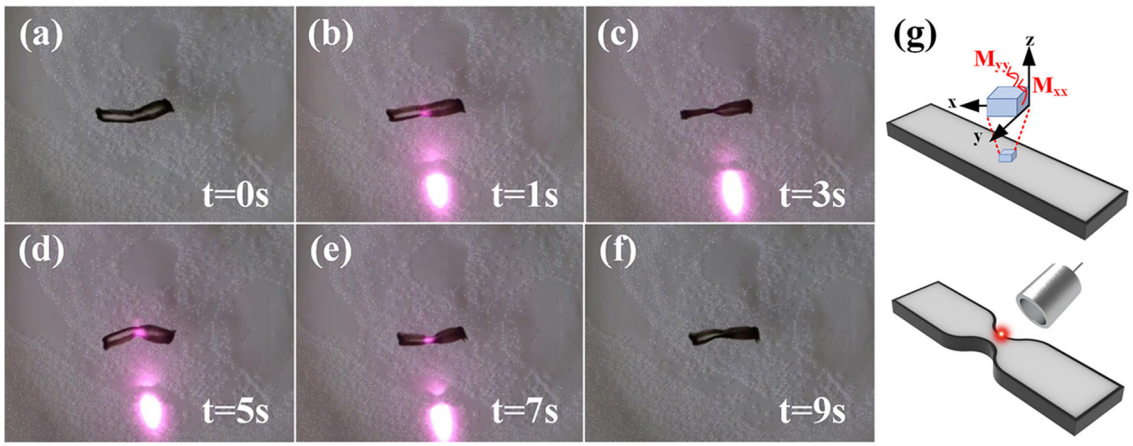

FIGURE 8 | The **(a–f)** multiple repetitive process and **(g)** a schematic diagram of rollover movement.

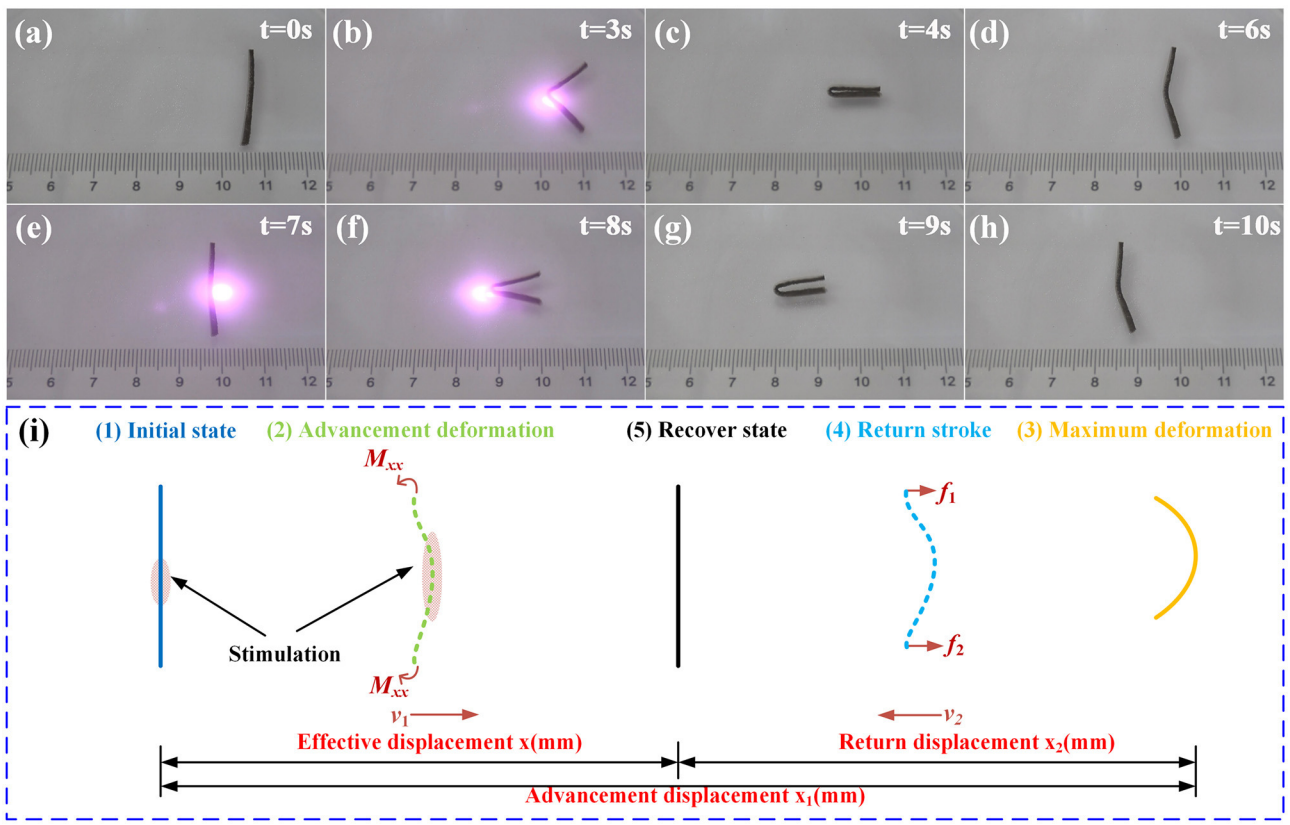

FIGURE 9 | The **(a–h)** multiple repetitive process and **(i)** a schematic diagram of forward movement.

another NIR irradiation cycle in **Figures 9e–g**, the NFC0 hydrogel actuator reached an effective displacement of 20 mm in **Figure 9h**. The forward movement process can be observed in **Supplementary Movie 6**. **Figure 9i** explains the forward movement mechanism on the base of the Foppl–von Karman elastic theory. Under NIR irradiation, the sample exhibited longitudinal and transverse deformation, which realized the advanced displacement of x_1 via the torque of M_{xx}. After removing irradiation, both ends of a sample acted as paddles leading to the backward motion. The hydrogel actuator exhibited a return displacement of x_2 via the forces of f_1 and f_2. The distance between the initial and recover states was an effective

displacement of forward movement. In addition to **Figures 7–9**, the prepared NFC0 and NFC2 hydrogel actuators realized controllable functional NIR-driven movements. Based on the hydrogels with different microstructures and Young's modulus, the hydrogel actuators exhibited different functional abilities.

Three-dimensional printing technology realized the precise, complicated 4D printed deformation structures of PNIPAm-XLG-NFC intelligent hydrogel actuators. The hydrothermal synthesized PNIPAm-4HBA-NFC intelligent hydrogel actuators owned the advantages of high response rate movement properties. Two kinds of intelligent hydrogel actuator owned distinct characteristics. The combination of advantages of different hydrogels can enrich the application fields of 4D printed hydrogel actuators in the field of soft intelligent actuator, artificial muscle, etc.

CONCLUSION

As a novel kind of reinforcement, NFC increased the crosslinking degree of intelligent hydrogels, which realized 3D printing of hydrogel reaction mixtures via the free radical polymerization under vacuum based on the improvement in the rheology property and increased Young's modulus of the hydrothermal synthesized hydrogels via a hydroxide radical on the dehydration synthesis between a monomer and crosslinking agent. The designed structure patterns affected NIR-driven deformation characteristics, which realized controllable deformations of saddle and inverted saddle based on the Model I and Model II, respectively. Attributed to a relatively high response rate and multiple deformation patterns, the hydrothermal synthesized intelligent hydrogel actuators were prepared. Based on the functional chemical bonds of NIPAm, the NFC0 and NFC2 intelligent hydrogels owned the specific volume phase transition temperatures, which built the material base for intelligent deformations combined with a typical network structure and the enhanced mechanical strength. Attributed to a unique structure design, the NFC0 and NFC2 intelligent hydrogels realized controllable functional movements. The wedge-shaped NFC2 intelligent hydrogel actuator pushed the resin ball with weight of 130 mg forward 8 mm in 39 s. Under the continuous NIR irradiation, the NFC0 hydrogel actuator realized controllable continuous rollover movement via the change of the torque values of the NFC0 hydrogel actuator on x-axis and y-axis. Based on the designed longilineal shape, the NFC0 hydrogel actuator realized forward movement, which reached an effective displacement of 20 mm in 10 s via two movement steps. The composition variation and structure design of a material were the key points of 4D printing. The hydrothermal synthesized intelligent hydrogel actuators owned abundant movement patterns and lacked a precise structure and mechanical strength. The combination of advantages of the 3D printed and hydrothermal synthesized intelligent hydrogel actuators provided a new development direction of 4D printing. The controllable NIR-driven deformations and functional pushball movement, rollover movement, and forward movement built abundant function bases for the practical applications of 4D printing in soft robot, drug delivery, and artificial muscle.

DATA AVAILABILITY STATEMENT

The original contributions presented in the study are included in the article/**Supplementary Material**, further inquiries can be directed to the corresponding author/s.

AUTHOR CONTRIBUTIONS

QZ performed investigation, experiments, processing data, and writing original draft. ZY performed mechanical analysis. YL performed methodology, resources, and review. LeR performed methodology and review. LuR performed methodology and supervision. All authors contributed to the article and approved the submitted version.

FUNDING

This work was supported by the Project of National Key Research and Development Program of China (2018YFB1105100, 2018YFC0703300, and 2018YFA2001300), the National Natural Science Foundation of China (Nos. 5167050531, 51822504, and 91848204), Key Scientific and Technological Project of Jilin Province (20180201051GX), Program for JLU Science and Technology Innovative Research Team (2017TD-04), Joint Fund of Ministry of Education for Equipment Pre-research (2018G944J00084), and China Postdoctoral Science Foundation (2020M670845).

SUPPLEMENTARY MATERIAL

The Supplementary Material for this article can be found online at: https://www.frontiersin.org/articles/10.3389/fmats.2021.661104/full#supplementary-material

REFERENCES

Fujigaya, T., Morimoto, T., Niidome, Y., and Nakashima, N. (2008). NIR laser-driven reversible volume phase transition of single-walled carbon nanotube/Poly(N-isopropylacrylamide) composite gels. *Adv. Mater.* 20, 3610–3614. doi: 10.1002/adma.200800494

Gladman, A. S., Matsumoto, E. A., Nuzzo, R. G., Mahadevan, L., and Lewis, J. A. (2016). Biomimetic 4D printing. *Nat. Mater.* 15, 413–439. doi: 10.1038/nmat4544

Hakan, A. N., Lee, A. K., and Yum, K. (2016). Bioinspired 3D structures with programmable morphologies and motions. *Nat. Commun.* 9, 3705–3716. doi: 10.1038/s41467-018-05569-8

Hu, Y., Liu, J. Q., Chang, L. F., Yang, L. L., Xu, A. F., Qi, K., et al. (2017). Electrically and sunlight-driven actuator with versatile biomimetic motions based on rolled carbon nanotube bilayer composite. *Adv. Funct. Mater.* 27, 1704388–1704397. doi: 10.1002/adfm.201704388

Jiang, W. T., Niu, D., Liu, H. Z., Wang, C. H., Zhao, T. T., Yin, L., et al. (2014). Photoresponsive soft-robotic platform: biomimetic fabrication and remote actuation. *Adv. Funct. Mater.* 24, 7598–7604. doi: 10.1002/adfm.201402070

Liu, X., Yuk, H., Lin, S., Parada, G. A., Tang, T. C., Tham, E., et al. (2017). 3D printing of living responsive materials and devices. *Adv. Mater*. 30, 1704821–1704829. doi: 10.1002/adma.201704821

Lo, C., Zhu, D., and Jiang, H. (2011). An infrared-light responsive graphene-oxide incorporated poly(N-isopropylacrylamide) hydrogel nanocomposite. *Soft Matter*. 7, 5604–5609. doi: 10.1039/c1sm00011j

Lu, S., and Panchapakesan, B. (2007). Photomechanical responses of carbon nanotube/polymer actuators. *Nanotechnology* 18, 305502–305510. doi: 10.1088/0957-4484/18/30/305502

Luo, R. C., Wu, J., Dinh, N. D., and Chen, C. H. (2015). Gradient porous elastic hydrogels with shape-memory property and anisotropic responses for programmable locomotion, *Adv. Funct. Mater*. 25, 7272–7279. doi: 10.1002/adfm.201503434

Must, B. I., Kaasik, F., Põldsalu, I., Mihkels, L., Johanson, U., Punning, A., et al. (2015). Ionic and capacitive artificial muscle for biomimetic soft robotics. *Adv. Eng. Mater*. 17, 84–94. doi: 10.1002/adem.201400246

Wang, E., Desai, M. S., and Lee, S. W. (2013). Light-controlled graphene-elastin composite hydrogel actuators. *Nano Lett*. 13, 2826–2830. doi: 10.1021/nl401088b

Wang, L., Liu, Y., Cheng, Y., Cui, X. G., Lian, H. Q., Liang, Y. R., et al. (2015). A bioinspired swimming and walking hydrogel driven by light-controlled local density. *Adv. Sci*. 2, 1500084–1500089. doi: 10.1002/advs.201500084

Wang, Y., Zhang, J. Y., Qiu, C. B., Li, J. B., Cao, Z. X., Ma, C. S., et al. (2018). Self-recovery magnetic hydrogel with high strength and toughness using nanofibrillated cellulose as a dispersing agent and filler. *Carbohyd. Polym*. 196, 82–91. doi: 10.1016/j.carbpol.2018.05.023

Weissleder, R. (2001). A clearer vision for *in vivo* imaging. *Nat. Biotechnol*. 19, 316–317. doi: 10.1038/86684

Xue, L. J., Kovalev, A., Volf, A. E., Steinhart, M., and Gorb, S. N. (2015), Humidity-enhanced wet adhesion on insect-inspired fibrillar adhesive pads. *Nat. Commun*. 6, 6621–6629. doi: 10.1038/ncomms7621

Yao, C., Liu, Z., Yang, C., Wang, W., Ju, X. J., Xie, R., et al. (2015). Poly (N-isopropylacrylamide)-clay nanocomposite hydrogels with responsive bending property as temperature-controlled manipulators. *Adv. Funct. Mater*. 25, 2980–2991. doi: 10.1002/adfm.201500420

Zhang, E. Z., Wang, T., Hong, W., Sun, W. X., Liu, X. X., and Tong, Z. (2014). Infrared-driving actuation based on bilayer graphene oxide-poly(N-isopropylacrylamide) nanocomposite hydrogels. *J. Mater. Chem. A* 2, 15633–15639. doi: 10.1039/c4ta02866j

Zhao, Q., Chang, Y. J., Yu, Z. L., Liang, Y. H., Ren, L., and Ren, L. Q. (2020). Bionic intelligent soft actuators: high-strength gradient intelligent hydrogels with diversified controllable deformations and movements. *J. Mater. Chem. B* 8, 9362–9373. doi: 10.1039/D0TB01927E

Zhao, Q., Liang, Y. H., Ren, L., Qiu, F., Zhang, Z. H., and Ren, L. Q. (2018a). Study on temperature and near-infrared driving characteristics of hydrogel actuator fabricated via molding and 3D printing. *J. Mech. Behav. Biomed*. 78, 395–403. doi: 10.1016/j.jmbbm.2017.11.043

Zhao, Q., Liang, Y. H., Ren, L., Yu, Z. L., Zhang, Z. H., Qiu, F., et al. (2018c). Design and fabrication of nanofibrillated cellulose-containing bilayer hydrogel actuators with temperature and near infrared laser responses. *J. Mater. Chem. B* 6, 1260–1272. doi: 10.1039/c7tb02853a

Zhao, Q., Liang, Y. H., Ren, L., Yu, Z. L., Zhang, Z. H., and Ren, L. Q. (2018b). Bionic intelligent hydrogel actuators with multimodal deformation and locomotion. *Nano Energy* 51, 621–631. doi: 10.1016/j.nanoen.2018.07.025

Conflict of Interest: The authors declare that the research was conducted in the absence of any commercial or financial relationships that could be construed as a potential conflict of interest.